Journal of Materials Research and Technology 41 (2026) 2383–2398

Contents lists available at ScienceDirect

Journal of Materials Research and Technology

journal homepage: www.elsevier.com/locate/jmrt

Evaluation of microscopy techniques to analyze the interphase of *Schizolobium amazonicum* glued-laminated timber with different adhesives

Raquel Schmitt Cavalheiro [a,*], Pedro Ignácio Lima Gadêlha Jardim [b], Antônio José Santos Junior [c], Victor Almeida de Araújo [d], Carlito Calil Júnior [a], Francisco Antonio Rocco Lahr [a], Afonso Rangel Garcez de Azevedo [e], Sergio Neves Monteiro [f], André Luis Christoforo [c]

[a] Department of Structural Engineering, University of São Paulo, São Carlos, Brazil
[b] Department of Civil Engineering, Federal University of Rondônia, Porto Velho, Brazil
[c] Department of Civil Engineering, Federal University of São Carlos, São Carlos, Brazil
[d] Postgraduate Program in Civil Engineering, São Paulo State University, Ilha Solteira, Brazil
[e] Civil Engineering Laboratory, State University of Northern Rio de Janeiro Darcy Ribeiro, Brazil
[f] Military Engineering Institute, Rio de Janeiro, Brazil

ARTICLE INFO

Keywords:
Paricá
Glued laminated timber
Bonding quality
Microstructural analysis
Microscopy techniques
Wood adhesion

ABSTRACT

The use of hardwood species in glued laminated timber (glulam) production enables the utilization of native resources, with Paricá (*Schizolobium amazonicum*) showing promising properties comparable to commonly used species in Brazil. The structural performance of glulam beams is strongly influenced by the quality of the interface, which is often assessed through macroscale tests. However, microscopic evaluation of the glue line is essential to fully understand bonding characteristics affecting performance. Despite the availability of several microscopy techniques, including polarized light microscopy (LM), fluorescence microscopy (FM), confocal laser scanning microscopy (CSLM), scanning electron microscopy (SEM), and X-ray microtomography (microCT), comparative studies on their effectiveness for glulam characterization are rare. This study compares five microscopy techniques for evaluating adhesive penetration in Paricá glulam, analyzing three different adhesives. Results indicate that the microscopy methods are complementary, with each offering distinct advantages and limitations. Notably, microCT and CSLM provided the most comprehensive details about the glue line. The research presents a comparative overview and suggests a protocol for microscopy-based characterization of glued interfaces. To enhance assessment of bonding quality, it is recommended that, beyond conventional macroscale tests, at least two complementary microscopy analyses be carried out for a more complete structural evaluation of glulam beams.

1. Introduction

Glued laminated timber (glulam) is a massive engineered product composed of timber lamellae arranged in parallel and bonded with adhesives that provide high strength and stability, making it widely used in large-span structures and prominent architectural projects [1]. Generally, these elements are produced from pine and eucalyptus timber [2,3]. However, the pursuit of better utilization of forest diversity, especially in countries with tropical climates, has encouraged investigations into other species, aiming to strengthen local production chains and expand access to sustainable raw materials [4,5].

In this context, Paricá (*Schizolobium amazonicum*) stands out as a promising alternative due to its rapid growth, widespread distribution in the North and Northeast regions of Brazil, and favorable processing characteristics. It is a lightweight, soft timber with a coarse texture and reddish-cream coloration, presenting a low incidence of defects and knots, which facilitates industrial sawing. Despite its low natural durability against biological agents, Paricá has reduced density (ranging

* Corresponding author.
E-mail addresses: raquelschmitt1@gmail.com (R.S. Cavalheiro), eng.pedrojardim@gmail.com (P.I. Lima Gadêlha Jardim), antoniojsj@estudante.ufscar.br (A.J. Santos Junior), va.araujo@unesp.br (V. Almeida de Araújo), calil@sc.usp.br (C.C. Júnior), frocco@sc.usp.br (F.A. Rocco Lahr), afonso@uenf.br (A.R. Garcez de Azevedo), snevesmonteiro@gmail.com (S.N. Monteiro), alchristoforo@ufscar.br (A.L. Christoforo).

https://doi.org/10.1016/j.jmrt.2026.01.171
Received 4 December 2025; Received in revised form 12 January 2026; Accepted 22 January 2026
Available online 23 January 2026

from 262 kg/m^3 in 5-year-old trees to 303 kg/m^3 in 11-year-old trees) and physical and mechanical properties comparable to those of pine species widely used in the construction industry, such as *Pinus elliottii* and *Pinus taeda* [6,7] thus offering potential to diversify the raw-material base and reduce pressure on the use of plantation-grown species traditionally adopted for structural applications.

Despite this potential, there is a notable gap in the literature regarding the use of Paricá in glulam elements. A systematic search in the Scopus and Web of Science databases, using the string (“glued laminated timber” OR “glulam”) AND (“parica” OR “schizolobium amazonicum”), identified only five related publications. Additionally, three further references were found, totaling eight publications on the subject. Studies have investigated the structural behavior of Paricá glulam beams manufactured with different adhesives, focusing on stiffness/strength response at the beam level [8–10]. Bonding quality has also been directly assessed through glue-line performance indicators such as shear strength and delamination, providing evidence on adhesive effectiveness in Paricá laminations [11]. In addition, preservative-related effects have been examined by comparing CCA treatment routes applied before bonding or after beam assembly, and their implications for flexural response and bondline integrity [12]. Other efforts have explored methodological aspects for determining or using modulus of elasticity in lamella grading and beam layup strategies [13]. More application-driven studies evaluated reinforcement solutions using glass- and carbon-fiber composites to enhance bending stiffness/strength [14], while joint-related investigations examined the influence of scarf-joint geometry (different angles) on the mechanical performance of Paricá glulam beams [15]. Despite the valuable contributions of these studies, significant gaps remain, particularly regarding the microstructural characterization of the bonding region, adhesive penetration behavior, and the adhesive interface in these engineered structures.

Understanding the performance of the glue line in engineered timber structures depends crucially on the microscopic properties of this system. Adhesive penetration occurs at multiple scales within the interface region and is influenced by the adhesive's ability to enter surface voids or penetrate the cell wall itself [16,17]. Macroscale tests provide important information for the overall assessment of elements; however, they are insufficient to elucidate phenomena occurring at the microscopic scale, which directly impact structural performance [18,19].

A systematic search was conducted in the Scopus and Web of Science databases using the string ("glued laminated timber" OR "glulam") AND (“microscopy” OR “microtomography”), which resulted in the identification of eleven articles focused on the use of microscopy and imaging techniques in the analysis of glulam elements. Optical/polarized light microscopy has been mainly used to describe the morphology of the pure bondline (e.g., glue-line continuity/thickness and visible defects) and to support qualitative comparisons between manufacturing conditions [19–21]. Fluorescence microscopy, often combined with confocal scanning laser microscopy, provides improved contrast for mapping adhesive distribution and estimating penetration depth at the interface, while confocal imaging further enables observation of penetration at the cellular scale; nevertheless, these approaches commonly rely on fluorescent labeling and may be affected by limited depth of field (FM) or shadowing on irregular surfaces (CSLM) [19]. Scanning electron microscopy is the most frequent technique in the retrieved literature, supporting high-resolution assessment of bondline morphology, lumen filling, microdamage accumulation, and failure mechanisms under thermal or mechanical actions, although grayscale imaging may hinder clear differentiation between wood and adhesive phases [18,21–27]. More recently, X-ray microtomography (microCT) has enabled non-destructive three-dimensional evaluation of adhesive distribution and voids along the bondline, allowing quantitative comparisons between conditions, albeit often requiring contrast enhancement for reliable segmentation of the adhesive phase [28].

However, there is a lack of studies aimed at performing a comparative analysis of the effectiveness of these techniques for characterizing the bonding region in glulam beams, especially regarding the use of tropical species such as Paricá. Recent studies indicate that combining multiple microscopy techniques can provide a more detailed understanding of the mechanical performance of the bonding interface [19], although methods present particularities regarding resolution, sample complexity, scope of information generated, and associated costs.

Given this context, the present work sought, to the best of our knowledge for the first time, to analyze the bondline region of Paricá glulam beams using five microscopy techniques. Rather than contrasting microscopic analyses with mechanical assessment, this study adds a microstructural layer to the conventional performance evaluation by examining how each imaging method reveals bondline features and adhesive penetration. Because penetration metrics are strongly technique and orientation-dependent, the microscopy comparison is presented mainly on a qualitative basis. The work discusses the capabilities and limitations of each technique and proposes guidelines to support industrial micro-level quality control of the bonding process, thereby contributing to the sustainable and technologically robust use of Paricá in engineered timber construction systems.

2. Material and methods

2.1. Materials

In this study, Paricá timber treated by vacuum-pressure impregnation in an autoclave with CCA preservative (chromated copper arsenate), composed of chromium trioxide, cupric oxide, and arsenic pentoxide, was used. The lamellae were treated with CCA prior to bonding to reflect the intended service condition and common industrial practice for protected structural timber in the application context of this study. CCA is a water-soluble, viscous, brown-colored preservative product that is widely used commercially for timber protection in Brazil [12]. The preservative treatment was carried out by the company Usiprema Usina de Preservação de Madeira Comércio e Serviços LTDA ME, Ribeirão Bonito Unit, using the full-cell process, a method recommended for water-soluble preservatives.

Three commercial structural adhesives were used for bonding the lamellae: (i) a one-component polyurethane-based (PU) adhesive (Purbond HB S309, Henkel), which cures through a reaction with the moisture present in the timber, promoting suitable penetration and efficient formation of the glue line [29]; (ii) a two-component phenol-resorcinol-formaldehyde (PRF) adhesive (Cascophen RS-216-M/FM-60-M, Momentive [30]), selected for its high resistance to water, organic solvents, biological attack, moisture, and heat, making it suitable for applications exposed to the elements; and (iii) a melamine-urea-formaldehyde (MUF) adhesive, which requires a catalyst to initiate the curing reaction [31].

For microscopic analyses, staining and contrast agents were employed to enhance the distinction of the observed structures. In optical staining, Safranin O (Aldrich, 97 % purity), a cationic dye effective for differentiating woody cell structures, was used. In the micro-computed tomography tests, phosphotungstic acid (Vetec, analytical grade) was used as a contrast agent, optimizing the visualization of regions with variations in electron density.

2.2. Preparing the glulam beams

Six glulam beams were manufactured for each adhesive, measuring 300 cm in length, 10 cm in width, and 9 cm in thickness, totaling 18 beams. The adopted procedures are illustrated in Fig. 1. The lamellae (3 $\times$ 10 $\times$ 300 cm^3) were initially evaluated through visual grading according to the criteria established in ABNT NBR 7190-2 [32], with the lowest-stiffness lamella placed in the core of the beam and the higher-MOE lamellae positioned on the outer faces. Subsequently, static

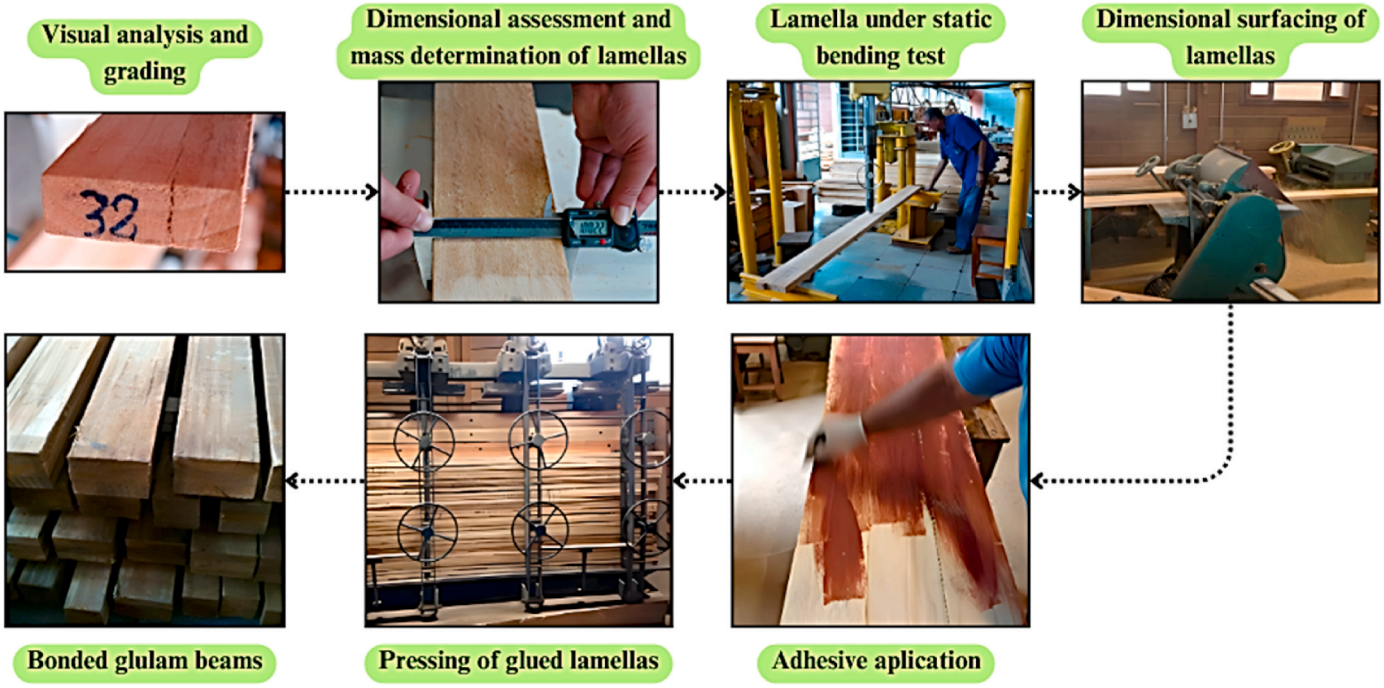

Fig. 1. Flow of stages of the glulam beam manufacturing process.

bending tests were performed to determine the modulus of elasticity (MOE) of each lamella. The average MOE of the lamellae used in the beams was 8208 MPa (CV = 13.7 %).

Each glulam beam was composed of three lamellae. The distribution of laminations within each beam was determined based on the measured MOE values, with the lamination exhibiting the lowest stiffness placed at the beam's central region, and those with higher MOE allocated to the outermost positions. This arrangement was adopted to enhance structural performance. The surfaces of the laminations were prepared by planning and cleaning. Each adhesive was applied with a brush to both contact surfaces, strictly adhering to the technical specifications (ideal glue-line spread) provided by each manufacturer, as detailed in Table 1. The gluing process was carried out within 24 h of the lamination preparation.

The pressing process was conducted with pressure and time parameters adjusted according to the manufacturer's recommendations for each adhesive system. Prior to bonding, all lamellae were conditioned and stored in the same sheltered and ventilated environment, protected from weather exposure, to promote moisture equilibration. According to Paris and Kamke [16], the lamellae must exhibit a moisture content of 12 % and be freshly planed at the time of bonding, a condition necessary to ensure adhesive quality.

2.3. Evaluation of the mechanical performance of glulam beams

The procedures used to assess the mechanical performance of the glulam beams are illustrated in Fig. 2. After the bonding process, the beams were subjected to static bending tests, with a concentrated load applied at the center of the span. Deflection was monitored using a digital dial gauge with a resolution of 0.01 mm, installed at the point of maximum displacement.

For the determination of the MOE and MOR, six full-size glulam beams per adhesive type tested. The actual cross-section dimensions of each beam were measured using a digital caliper (0.01 mm precision), and the total length was measured with a steel tape.

The maximum deflection corresponding to the elastic regime was defined by the ratio L/300, where L is the clear span between supports. With a span of 2.30 m, the adopted allowable deflection was 7.6 mm. The MOE was calculated using Equation (1).

$$MOE = \frac{P \cdot L^3}{48 \cdot f_{max} \cdot I} \quad (1)$$

Where MOE represents the modulus of elasticity (MPa); P is the load applied at mid-span (N); f_{max} is the deflection or displacement resulting from the application of the load (mm); and I denote the moment of inertia of the beam (mm^4) relative to the bending axis. The flexural strength of the beams (Equation (2)), expressed by the modulus of rupture (MOR), was calculated from the ratio between the maximum bending moment (N·mm) and the flexural section modulus (mm^3).

$$MOR = \frac{M}{W} \quad (2)$$

Specimens for shear testing were obtained from the same glulam beams previously tested in static bending. In the shear tests, six specimens per adhesive type were prepared so that the wood fibers remained parallel to the direction of the applied load. The contact surfaces were kept flat and parallel to each other. A notch was made at one end of the specimen, while the other end received a continuous transverse cut across the entire thickness of the layer, reaching the glue line. The tests were performed on an AMSLER-type universal testing machine, operating in compression mode, with the load applied according to the parameters specified by the CSA 0112.9 [33].

Delamination specimens were subsequently cut from those beams following the bending tests. For the evaluation of delamination resistance, six specimens per adhesive type were initially conditioned in an environment at 20 ± 2 °C and 65 ± 5 % relative humidity for two days

Table 1
Adhesive application specification.

Adhesive	Manufacturer		Adopted	
	Spread rate (g/m^2)	Gluing pressure (kPa)	Spread rate (g/m^2)	Gluing pressure (kPa)
MUF	250–400	1000	350	1000
PRF	60–216	1000–1400	200	1200
PU	140–180	600–1000	150	800

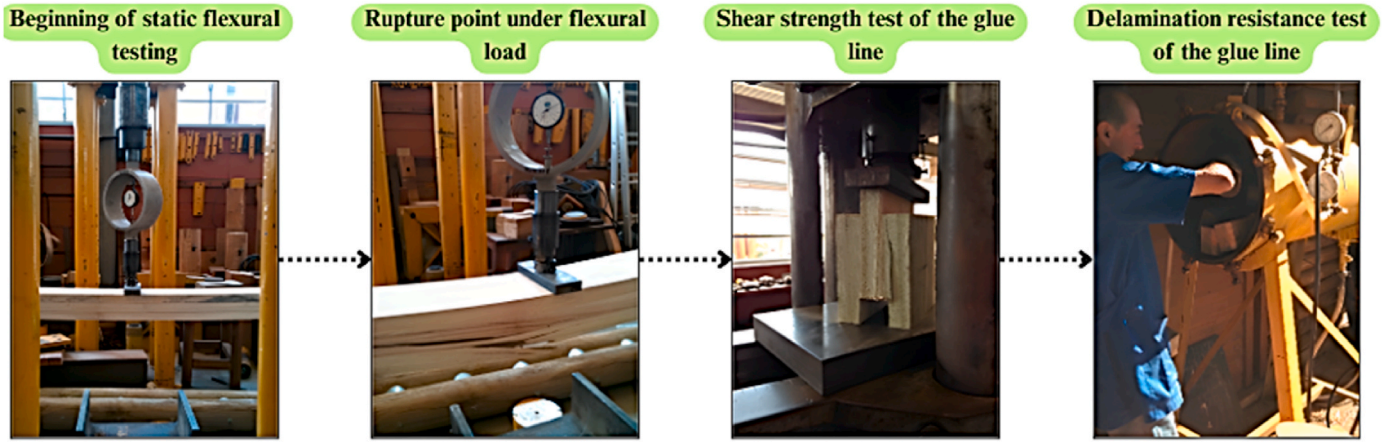

Fig. 2. Flow of tests performed for mechanical characterization.

[28,34,35]. After this period, the samples were cut to a width of 7.5 cm, with their length adjusted to the same dimension. The pieces were then arranged in an autoclave with spacers, ensuring that the upper faces remained exposed to humidity and fully submerged with the aid of weights.

The test sequence followed cycles of controlled pressure. First, a pressure of 75 ± 10 kPa was applied for 2 h with water at 22 ± 5 °C. Subsequently, the pressure was raised to 540 ± 20 kPa for an additional 2 h. Afterwards, the samples were subjected to a drying process at 28 ± 2 °C for 88 h under forced ventilation, until they reached a mass equivalent to 5–6 % of their initial weight. The complete 96-h cycle was repeated twice. At the end of the test, the total length of visible delamination along the glue lines was measured to a precision of 0.1 cm, disregarding any delamination shorter than 0.25 cm, following procedures adopted in other studies [36–38].

2.4. Preparing samples for microscopic analysis

Ten samples per adhesive type, intended for microscopic analyses, were extracted from the beams, forming specimens with a maximum thickness of 1 cm, with base and height adjusted to the dimensions of each element. These same sampling units served as the common source material for all microscopy/imaging techniques (LM, FM, CSLM, SEM, and microCT). When a given method required specific preparation, dedicated sub-samples were derived from the same sampling units, ensuring full traceability across methods, although not necessarily using the exact same physical piece in every technique. From these pieces, approximately cubic sections measuring 1 × 1 × 1 cm^3 were obtained, compatible with the analysis equipment. Subsequently, the samples were dried in a vacuum oven for 72 h at 40 °C. This procedure aimed solely at moisture removal and did not intend to stabilize or alter the wood microstructure before microtome sectioning.

The final sectioning of the samples was performed using a Leica RM2255 rotary microtome at the Department of Materials Engineering, EESC/USP, allowing for the preparation of regular and precise surfaces for optical and electron analysis. Part of the samples was prepared for observation by polarized light optical microscopy (LM), fluorescence light microscopy (FM), and confocal scanning laser microscopy (CSLM), with and without staining with Safranin O. LM was performed using the Leica DM2700 M system with LED illumination, also at EESC/USP. Fluorescence analyses were conducted using the Labomed Lx 400 microscope with an iVu 5000 camera at the São Carlos Institute of Physics (IFSC/USP), with excitation in the blue range. Confocal images were acquired with the Zeiss LSM 780 inverted confocal microscope, operating with an argon laser at 458 nm and emission at 504 nm. Data processing and analysis were carried out using ZEN 2.3 software (Blue Edition, 2011) at the Multiuser Laboratory of São Carlos Institute of Physics of the University of São Paulo.

For the non-destructive three-dimensional characterization of adhesive penetration, microCT was performed using a SkyScan 1272 (Bruker) system installed at the High-Resolution Spectroscopy Laboratory of IFSC/USP. The system was operated at 50 kV and 200 μA, with a resolution of 3.5 μm. Volumetric reconstruction was carried out using NRecon software, and segmentation of the adhesive/timber phases was performed in PerGeos.

Samples intended for SEM analysis were mounted with conductive tape onto metal stubs, with special care taken to avoid damage during dry mounting. Gold coating was applied by sputtering using the Quorum Q150 R ES system. High-resolution images of the glue line were obtained with the Inspect F50 SEM, located at EESC/USP, operated at an accelerating voltage of 10 kV. A Fig. 3 illustrates the sample preparation procedure and the equipment used.

3. Results and discussion

3.1. Mechanical performance

Table 2 presents the mean values, coefficients of variation (CV, in parentheses), and the results of Tukey's mean contrast test obtained from the mechanical tests of the glulam beams for the different types of adhesives studied. The parameters evaluated were the modulus of elasticity (MOE), modulus of rupture (MOR), shear failure region, and the percentage of delamination observed in the glue lines.

It was observed that beams bonded with PRF adhesive exhibited higher values for both MOE and MOR compared to the others. Beams with MUF and PU adhesives also showed satisfactory performance in comparison with other studies [8,9]. Notably, no delamination (0 %) was observed in any of the samples analyzed, indicating the efficiency of the bonding process and good compatibility of the adhesive systems used with the wood substrate. Furthermore, in all cases, shear failure occurred exclusively in the timber, as also reported in other studies [9–11], demonstrating that the glue line surpassed the strength of the wood itself, a result considered ideal for structural applications [39,40]. In this regard, it is worth mentioning the study by Molina et al. [20], who evaluated similar adhesives applied to species such as pine and eucalyptus and observed delamination rates ranging from 0.63 % to 7.21 %. Although the cited studies were conducted on different wood species, their qualitative observations are consistent with the bonding behavior observed here. Therefore, our results for Paricá glulam indicate that bonding quality is governed by the adhesive system and pressing parameters and is strongly mediated by the timber microstructure.

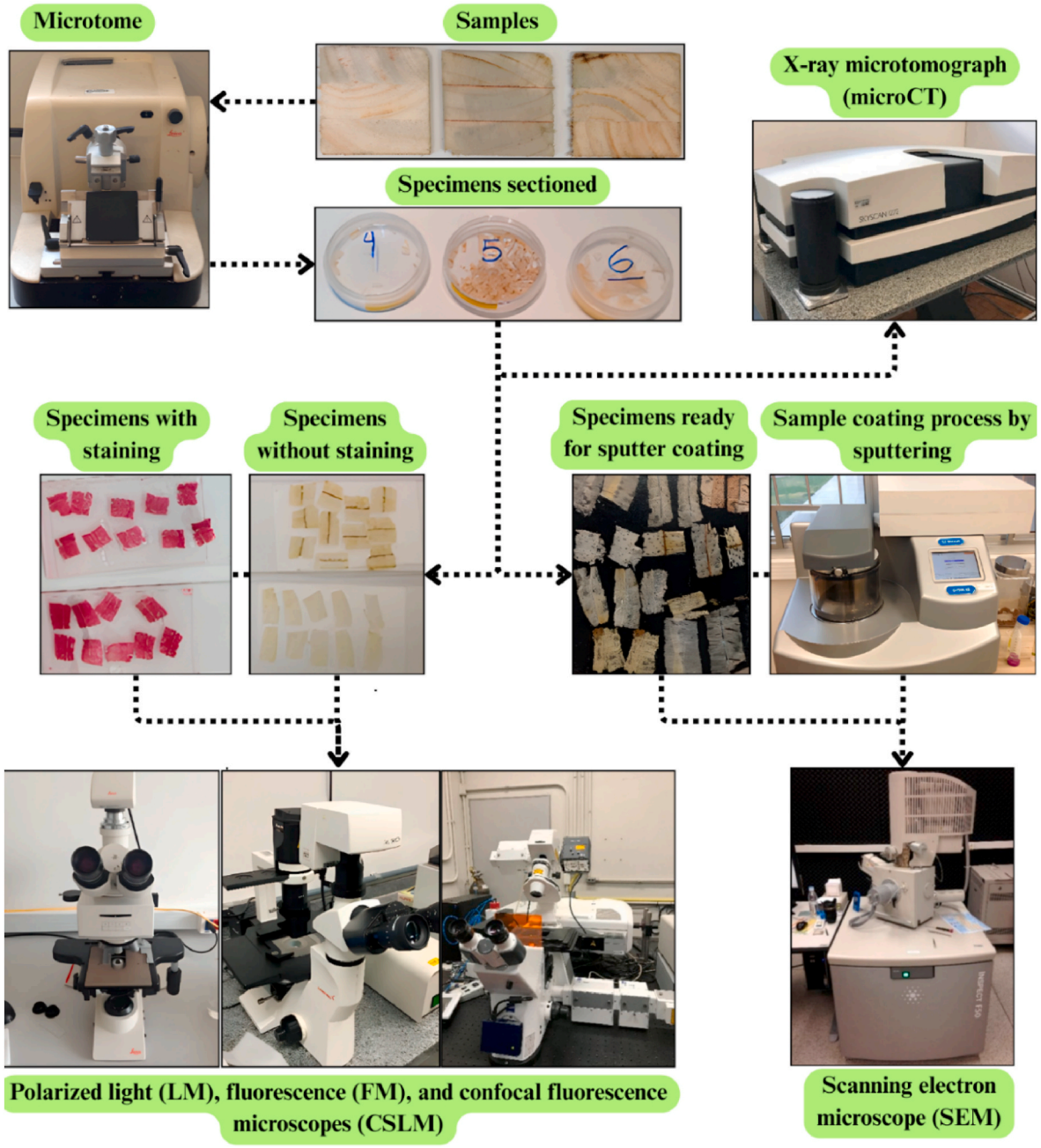

Fig. 3. Flow of stages of sample preparation for microscopy analyses.

Table 2
Mechanical test results.

Adhesive	MOE (MPa)	MOR (MPa)	Shear rupture region	Delamination (%)
MUF	7747^{B} (7.23 %)	41.0^{B} (12.45 %)	Timber (100 %)	0
PRF	8743^{A} (9.73 %)	57.7^{A} (16.24 %)	Timber (100 %)	0
PU	7786^{B} (6.36 %)	40.9^{B} (10.76 %)	Timber (100 %)	0

*According to Tukey's test (5 % significance level), "A" denotes the treatment associated with the highest mean value, "B" to the treatment with the second highest mean value, and identical letters indicate treatments with means that are statistically equivalent to each other.

3.2. Microscopy technique performance in bondline analysis

3.2.1. Polarized light optical microscopy (LM)

The analysis of the glue lines using polarized light optical microscopy was conducted before and after staining the wood with Safranin for all adhesives studied. One of the samples bonded with MUF adhesive is shown in Fig. 4.

In Fig. 4, which refers to the analysis of the bond lines formed by the MUF adhesive in Paricá lamellae, an absence of bubbles, residual stresses, or crystals is noted in the adhesive region, indicating satisfactory bonding quality and good adhesive-wood interaction. The cuts observed near the adhesive line are attributed to small cracks caused by the microtome during the preparation of the slides. A sample made with PRF adhesive is presented in Fig. 5.

Upon examining Fig. 5, the PRF adhesive, recognizable by its intense reddish coloration, can be easily identified in the adhesive line. No air

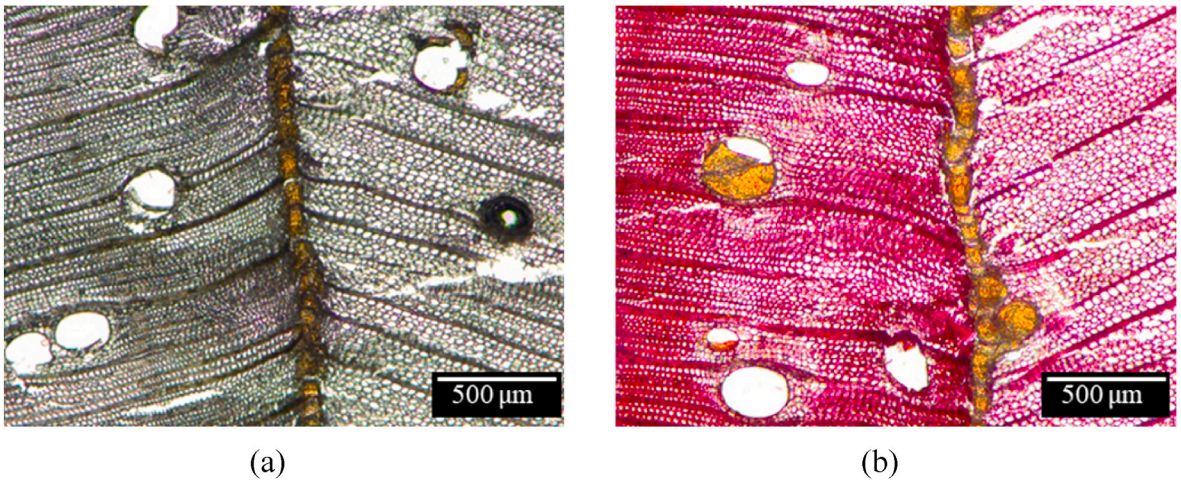

Fig. 4. LM analysis of MUF bondlines: (a) without dye; (b) with dye.

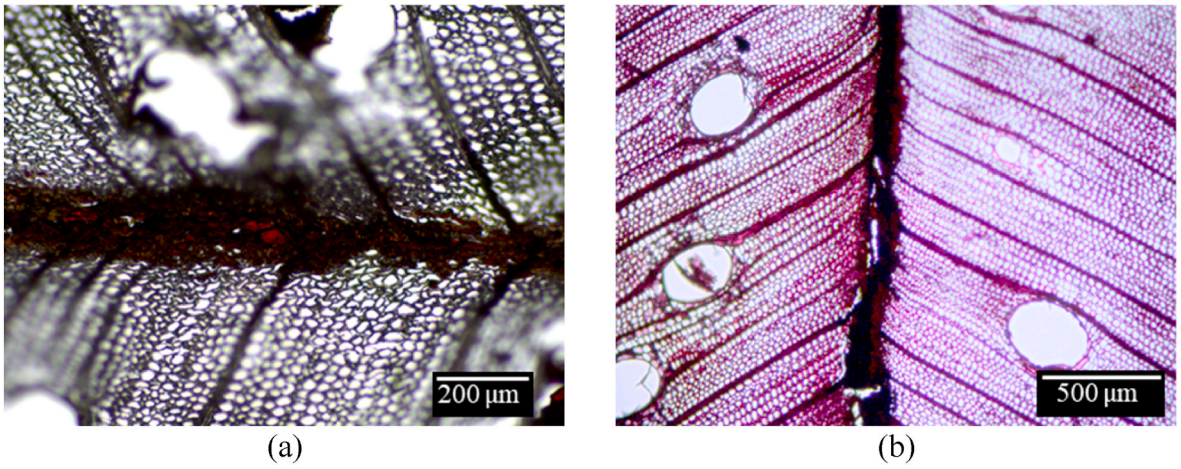

Fig. 5. LM analysis of PRF bondlines: (a) without dye; (b) with dye.

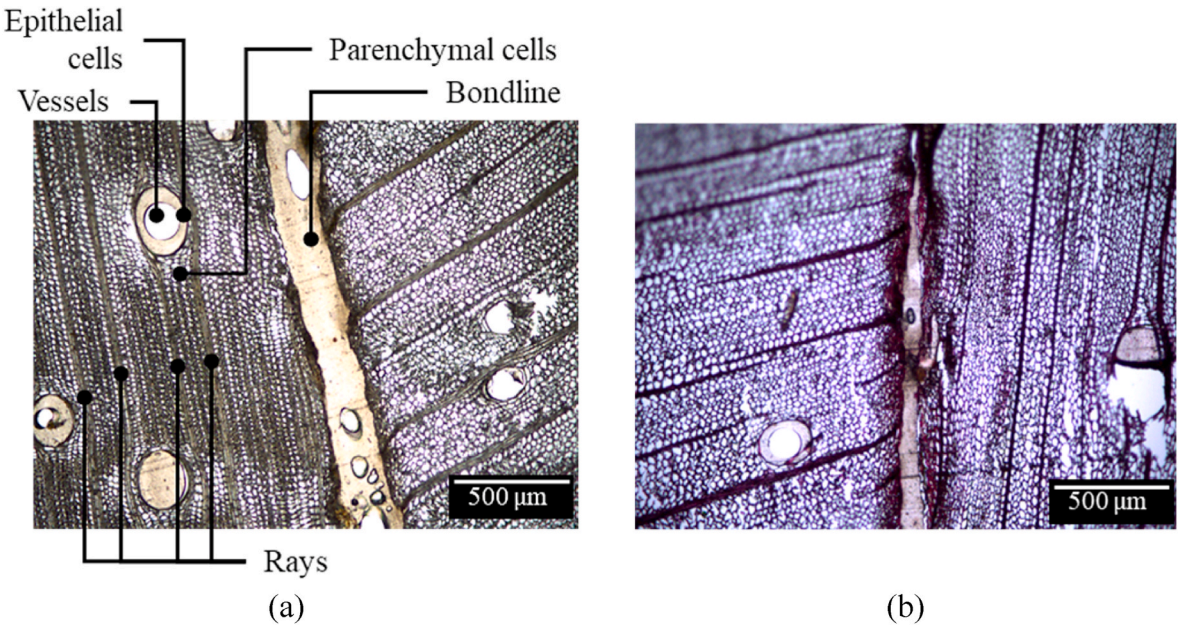

Fig. 6. LM analysis of PU bondlines: (a) without dye; (b) with dye.

bubbles, residual stresses, or crystal formation were observed. The application of Safranin and contrast adjustments were essential to distinguish anatomical details of the adhesive layer and wood cells. Small contour defects were also attributed to microtome sectioning, without hindering the evaluation of the bond line. A sample composed with PU adhesive is shown in Fig. 6.

In Fig. 6, the analysis of the glue line formed by the PU adhesive reveals the presence of microbubbles in the adhesive matrix, although no residual stresses or crystals were identified. Despite the occurrence of microbubbles, the final integrity of the bond was not compromised, as confirmed by the mechanical tests performed. Such microbubbles may be associated with the spontaneous expansion reaction characteristic of one-component PU adhesives, whose curing process generates gases such as CO_2. This feature is further accentuated in high-viscosity adhesives, such as Jowapur 686.60 (PU), used by Molina et al. [20], which can make uniform distribution more difficult and favor the formation of microscopic voids during application. However, the shear strength tests showed failures predominantly within the wood rather than at the glue line, indicating that the adhesive integrity was maintained. Similarly, Qin et al. [19] observed that, even in the presence of microcracks and imperfections in bonding regions, effective adhesive penetration into the cell walls was able to restore local mechanical properties, demonstrating that small discontinuities do not necessarily compromise the structural performance of the bond.

By observing the rays of the lamella on the left, they are positioned perpendicularly to those of the lamella on the right, reflecting the orientations adopted in cutting the pieces for beam assembly. Industrially, log cuts are performed to minimize waste and maximize wood utilization [41,42]. It is noteworthy that this situation is common in beams and can result in different adhesion outcomes.

3.2.2. *Fluorescence optical microscopy (FM)*

In this section, images obtained by fluorescence optical microscopy after the application of Safranin O are presented. It is noteworthy that, despite the staining strategy, the generated images exhibited low resolution and limited focus, which restricted detailed analysis of the wood-adhesive interface. However, it was still possible to identify the adhesive line thickness and penetration depth, as well as features such as bubble formation and lumen filling. A sample prepared with MUF adhesive is shown in Fig. 7.

In the images presented in Fig. 7 (MUF), it can be observed that the interface between the adhesive line and the wood tissue could not be clearly discerned due to the low resolution and limited depth of field. Some regions were identified where the adhesive line appears in its pure phase, with no indication of air bubbles or crystals, as well as vessels that are filled, likely by capillarity during adhesive application. In Fig. 7a, due to the lack of focus and low resolution, it is only possible to identify two filled vessels distant from the adhesive line, while in Fig. 7b, although with better focus and resolution, it is still only possible to see the adhesive line in its pure phase, and the interface cannot be analyzed.

It is also possible to observe a tear in the sample produced during microtome sectioning, which appears along the adhesive line. A sample composed with PRF adhesive is in Fig. 8.

The images presented in Fig. 8 show similar results for the PRF adhesive: even after staining, the low optical quality of the images limited the analysis of adhesive spreading and the adhesive interface. In Fig. 8a only the dark reddish adhesive line can be observed in the center of the image. In the vessel region, a more intense fluorescence is observed with a yellowish coloration, distinct from that of the PRF adhesive, which is dark red. One possible reason for this coloring may be light emission from components of the CCA. In Fig. 8b it can also only be stated that adhesive is present in its pure phase along the adhesive line. No air bubbles or crystals were identified. It was not possible to observe adhesive spreading into the wood from these results. A sample bonded with PU adhesive is in Fig. 9. In Fig. 9, referring to the analysis of the PU bond line, an optical performance comparable to the previous samples is observed, with low resolution, but evidencing both vessel filling and adhesive penetration into lumina and rays.

In both images, the presence of air bubbles is also observed, a common characteristic of polyurethane systems due to the expansion reaction during curing [20]. A Fig. 9a, at a scale of 500 μm, resulted in an image with little focus and low resolution, allowing only the identification of the adhesive line in its pure phase and vessel filling, while in Fig. 9b it was possible to differentiate filled lumina and the arrangement of wood rays, providing the best observation performance among the samples tested, although still below ideal for detailed interface analysis.

3.2.3. *Confocal optical microscopy (CLSM)*

The sample (after staining with Safranin O) prepared with MUF adhesive is in Fig. 10.

Confocal fluorescence microscopy allowed for clear observation of the morphology of the wood tissues and the distribution of adhesives along the bond lines. Under the operational conditions employed, it was possible to clearly distinguish the cell walls of the wood and the adhesive, owing to the contrast provided by Safranin O. It is noteworthy that CLSM was more effective at visualizing adhesive distribution within wood tissues than FM.

In Fig. 10a (scale of 200 μm), referring to the MUF adhesive, shadowed areas were observed that made interface analysis difficult. Nevertheless, the adhesive line was clearly identified, as well as the

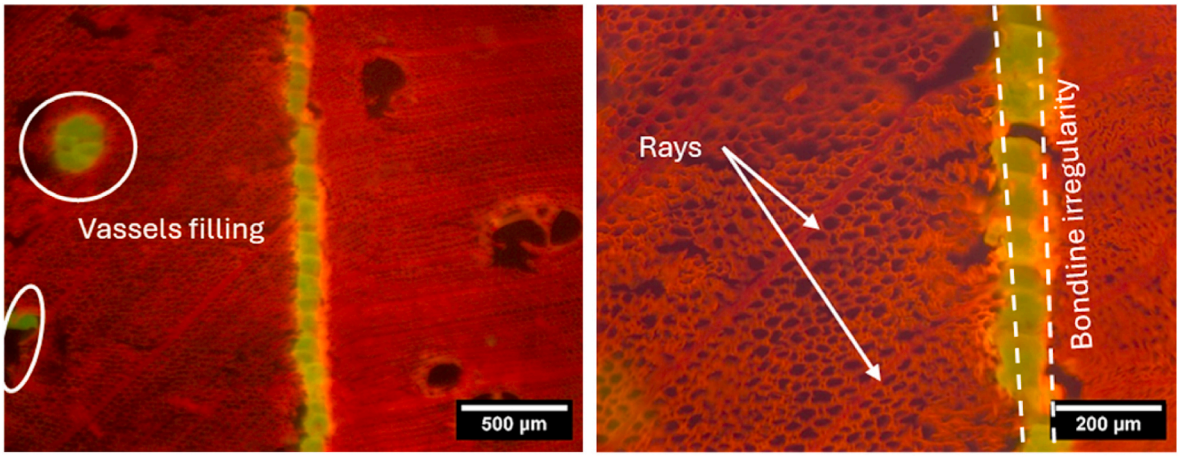

Fig. 7. FM analysis of MUF bondline: overview of the adhesive bondline (a) and detailed area of the bondline (b).

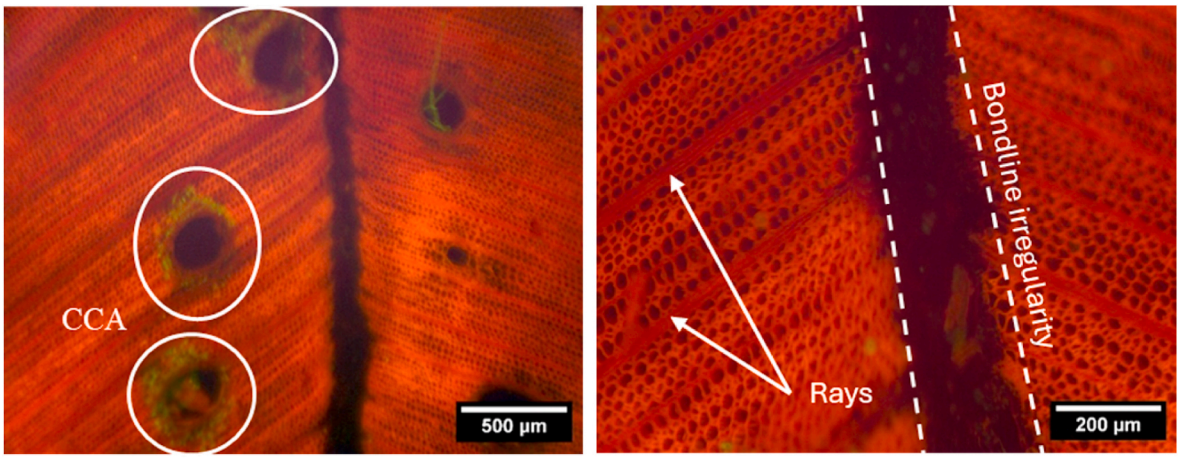

Fig. 8. FM analysis of PRF bondline: overview of the adhesive bondline (a) and detailed area of the bondline (b).

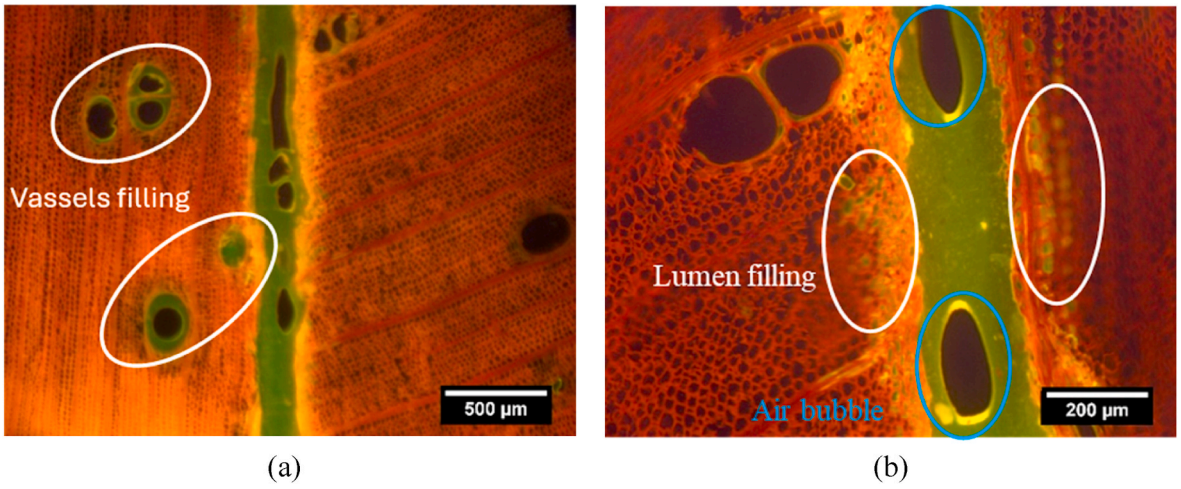

Fig. 9. FM analysis of PU bondline: overview of the adhesive bondline (a) and detailed area of the bondline (b).

filling of some vessels. In turn, Fig. 10b (scale of 50 µm), despite showing a smaller region, provided better visualization, with less shadow interference and revealed details such as damage to the adhesive line caused by microtome cutting, and the filling of rays and tracheid lumina. A sample composed with PRF adhesive is presented in Fig. 11.

In Fig. 11a, with PRF adhesive, it was possible to observe the adhesive filling some of the wood's rays and vessels. In Fig. 11b, the thickness of the adhesive line could be determined with good precision at approximately 100 µm, with the filling of rays also being highlighted. These findings are consistent with literature reports [19], which point to the greater precision of the confocal technique for quantitative analysis of adhesive penetration. A sample composed with PU adhesive is presented in Fig. 12.

In Fig. 12a (PU adhesive, with a scale of 200 µm), a clear identification was possible that the lamellae were cut and bonded in different orientations, as seen from the tissue patterns and the spread of adhesive following both structural pieces. Furthermore, the adhesive line in its pure phase was observed, as well as the filling of rays, vessels, and lumina. In Fig. 12b (scale of 100 µm), the formation of air bubbles, the intact adhesive line, and the filling of rays and lumina were clearly identified.

Based on our CLSM observations (with Safranin O staining), adhesive-dependent qualitative differences were noted in the bondline region. For MUF, shadowed areas occasionally hindered interface inspection, although the bondline and vessel filling were still identifiable (Fig. 10). For PRF, the adhesive filled rays and vessels and bondline thickness could be estimated with good precision (≈100 µm) in the detailed view (Fig. 11), consistent with reports that CLSM enables more precise micromorphological/quantitative inspection [19]. For PU, CLSM clearly revealed the pure adhesive phase, filling of rays/vessels/lumina, and the presence of air bubbles (Fig. 12).

Unlike FM, CLSM allowed for a more refined evaluation of the adhesive interfaces, overcoming the negative impacts of low resolution and lack of focus that limited previous analyses. It is important to highlight that, in the literature, CLSM is often mentioned as the method of choice for demanding micromorphological studies, thanks to its ability to produce high-resolution images with excellent color and structural discrimination [19,35].

3.2.4. *Scanning electron microscopy (SEM)*

This subsection presents the images obtained by scanning electron microscopy (SEM) of the adhesive lines produced with the different adhesives evaluated. The sample composed with MUF adhesive is shown in Fig. 13.

In Fig. 13a, an adhesive line with an approximate thickness of 100 µm is observed, along with the filling of vessels, despite multiple structural damages caused by microtome sectioning. This damage compromised part of the integrity of the sample, as shown in Fig. 13b,

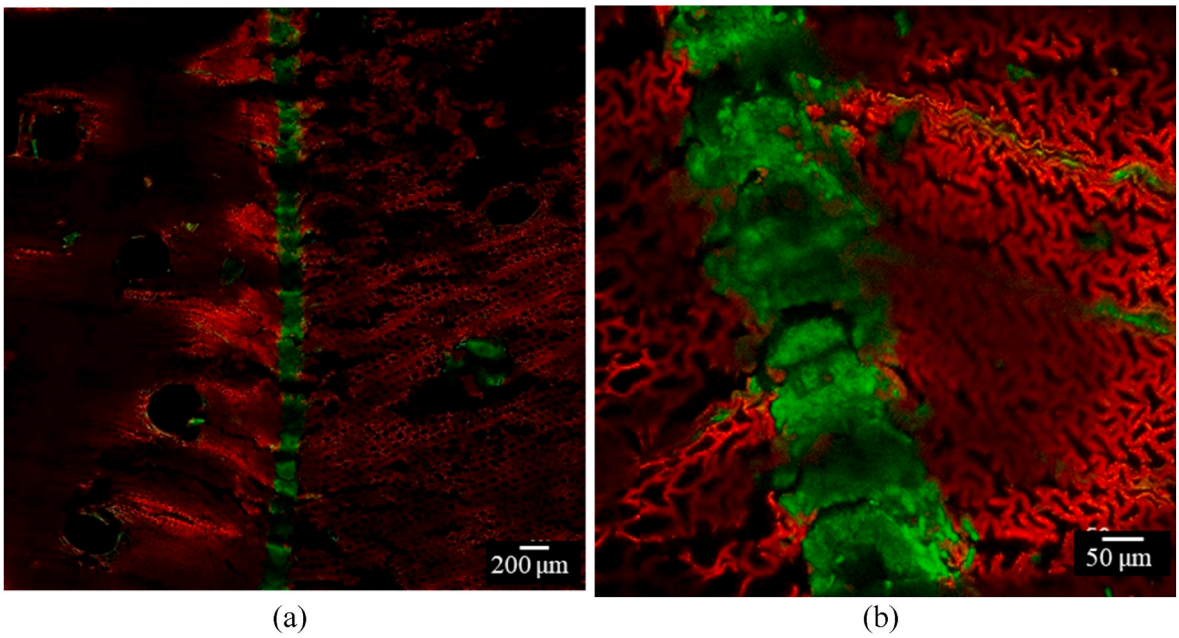

Fig. 10. CLSM analysis of MUF bondline: overview of the adhesive bondline (a) and detailed area of the bondline (b).

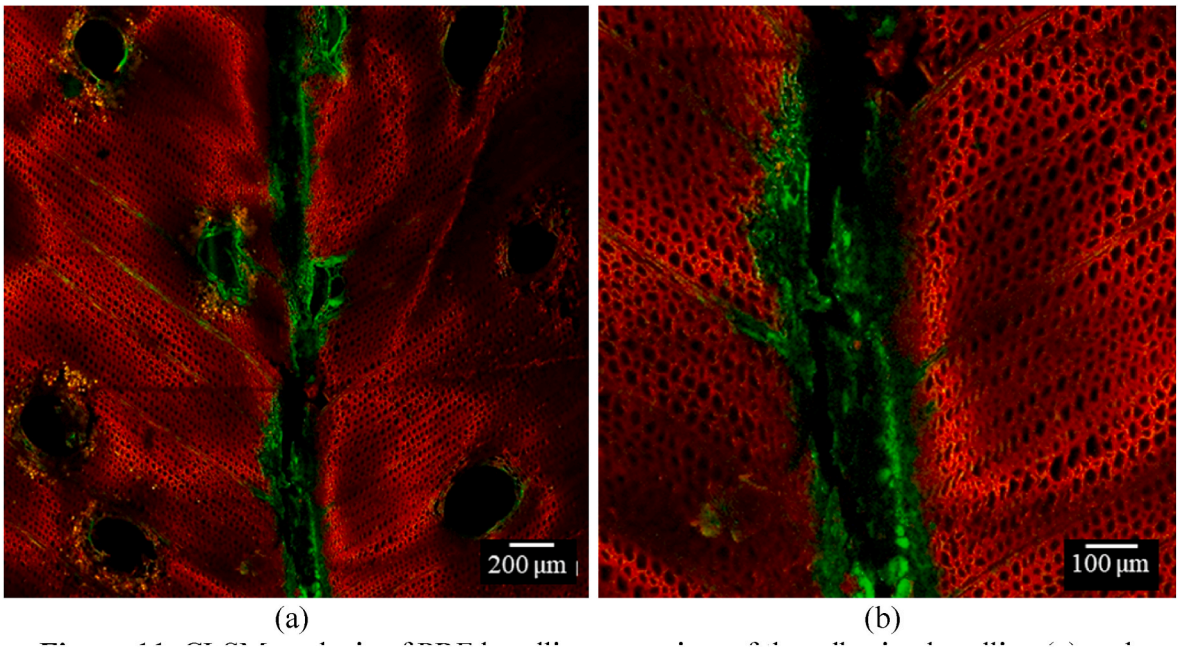

Fig. 11. CLSM analysis of PRF bondline: overview of the adhesive bondline (a) and detailed area of the bondline (b).

where the adhesive line is heavily damaged, leaving only a filled vessel visible with adhesive.

Fig. 13c (scale of 50 µm) highlights the fragility and thinness of the Paricá cell walls, typical of medium to low density woods. This characteristic significantly hindered sample preparation without causing additional ruptures. Even so, it is possible to identify lumina and vessels filled with adhesive.

Finally, Fig. 13d shows a wood ray filled with adhesive, suggesting its role in conducting the adhesive into the tissue and consequently filling the associated vessel. A sample composed with PRF adhesive is presented in Fig. 14.

In the images of Fig. 14, referring to the sample with PRF adhesive, it is observed that microtome sectioning, hindered by the low hardness of Paricá, caused significant damage to the samples, limiting the quality of the images and the detailed analysis of the adhesion. Even so, it is possible to distinguish the pure adhesive phase and the characteristic interface. A sample composed with PU adhesive is presented in Fig. 15.

In the images from Fig. 15, corresponding to the PU adhesive sample, the pure adhesive line stands out with a thickness of about 200 µm, in addition to adhesive penetration into tracheids, estimated at approximately 135 µm. The filling of lumina, vessels, and rays is also observed, highlighting the PU adhesive's performance in impregnating the wood cell structures.

Overall, SEM analysis enabled precise observation of the morphology of the adhesive lines, their interfaces, and the extent of penetration into different anatomical elements. However, the low hardness of Paricá

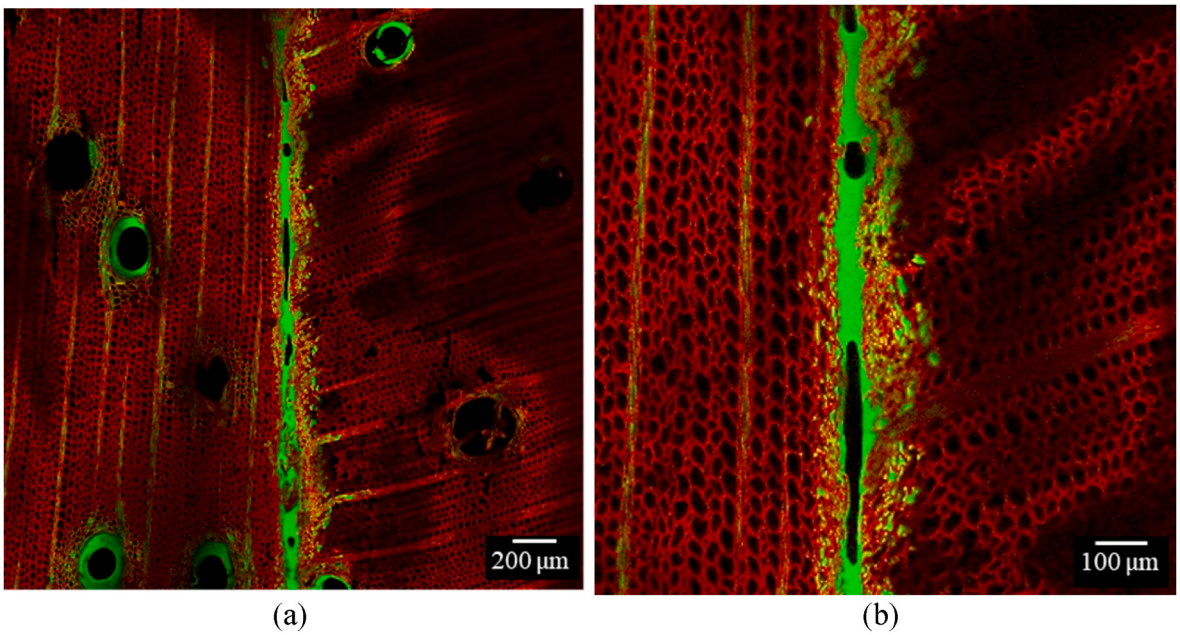

Fig. 12. CLSM analysis of PU bondline: overview of the adhesive bondline (a) and detailed area of the bondline (b).

wood posed significant challenges for sample preparation, resulting in damage that limited the evaluation of some parameters, especially in the analysis with PRF.

3.2.5. X-ray microtomography (microCT)

In this subsection, images obtained by micro-X-ray computed tomography (microCT) without the use of contrast agents are presented. It is important to note that this technique, when applied to organic materials, generally requires the use of contrast agents because the densities of the materials are very similar, as occurred in the case of these samples (adhesive and wood). The aim was to explore X-ray microtomography without the addition of contrast agents, since their inclusion could interfere with the adhesive curing process.

Despite this limitation, the technique proved efficient for quantifying the spread of the adhesive at the interface in three dimensions, especially due to the low density of the wood used. The sample composed with MUF adhesive is presented in Fig. 16.

In Fig. 16, a three-dimensional graphical reconstruction of the complete sample is observed, clearly displaying both the wood and the adhesive. The isolated visualization of the adhesive highlights its three-dimensional spread, with more pronounced penetration on one side of the sample and a predominance of vessel filling compared to lumina. The virtual section shown in the figure allows for the clear identification of the adhesive line located in the central region of the sample, as well as a filled vessel. The adhesive distribution graph confirms the asymmetric spreading and the uniformity of the pure phase, characterized by a single peak corresponding to the adhesive line. A sample composed with PRF adhesive is presented in Fig. 17.

In Fig. 17, the three-dimensional reconstruction highlights both the wood and the central adhesive line, as well as the adhesive spreading pattern. The isolated visualization of the adhesive demonstrates vessel filling, with little penetration into lumina, and shows a roughly symmetrical spread on both sides of the sample. The virtual section of the sample allows for clear visualization of the adhesive line and vessels filled with adhesive. Moreover, the distribution graph shows that the adhesive spread uniformly to both sides of the wood, with the adhesive line being relatively narrow. A sample composed with PU adhesive is presented in Fig. 18.

In Fig. 18, the three-dimensional reconstruction shows that the adhesive line is not centered relative to the sample cut. The three-dimensional visualization of the adhesive line highlights its asymmetric volumetric spread. The virtual section allows for a clear view of the adhesive line and a filled vessel. The distribution graph shows that the adhesive was distributed unevenly, with the adhesive line shifted away from the center of the sample.

3.3. Evaluation of bondlines

The analysis of the adhesive lines revealed that only the PU-based adhesive showed air bubbles in the pure phase of the line, while the MUF and PRF exhibited no evidence of bubbles, residual stresses, or crystals. The formation of bubbles in polyurethane systems is associated with the characteristic chemical reaction of this polymer in the presence of moisture. Among the reactions involved in polyurethane formation, the expansion reaction between isocyanate and water results in the formation of urea and carbon dioxide, whose diffusion produces bubbles and promotes expansion in the form of foam. This is an exothermic reaction, releasing about 47 kcal/mol of water. In the reaction of isocyanate with water, carbamic acid is first formed, which then decomposes into carbon dioxide and the corresponding amine; the amine immediately reacts with another molecule of diisocyanate, forming urea [18, 43].

Through the analysis of adhesive line thickness distribution in its pure phase, based on seven measurements taken along the bond line of samples for each adhesive, average thicknesses of 97.5 µm (CV = 27.34 %), 245.5 µm (CV = 24.91 %), and 113.6 µm (CV = 23.42 %) were obtained for samples bonded with MUF, PU, and PRF adhesives, respectively.

The results indicated that the adhesive lines in samples bonded with MUF have a significantly smaller thickness compared to the other adhesives. Across all samples, little filling of the tracheid lumina was observed. Analyses by polarized light optical microscopy also demonstrated compression of the tracheids at the interface, which can be attributed to the high pressure applied during beam pressing, a pressure that may have been excessive for Paricá wood, even when following the manufacturers' recommendations [44].

Another relevant aspect is the heterogeneity of the lamellae. In the samples bonded with MUF, one of the lamellae showed an interface with tracheids of larger radius, allowing greater adhesive penetration, while the other lamella was characterized by tracheids of smaller diameter, as

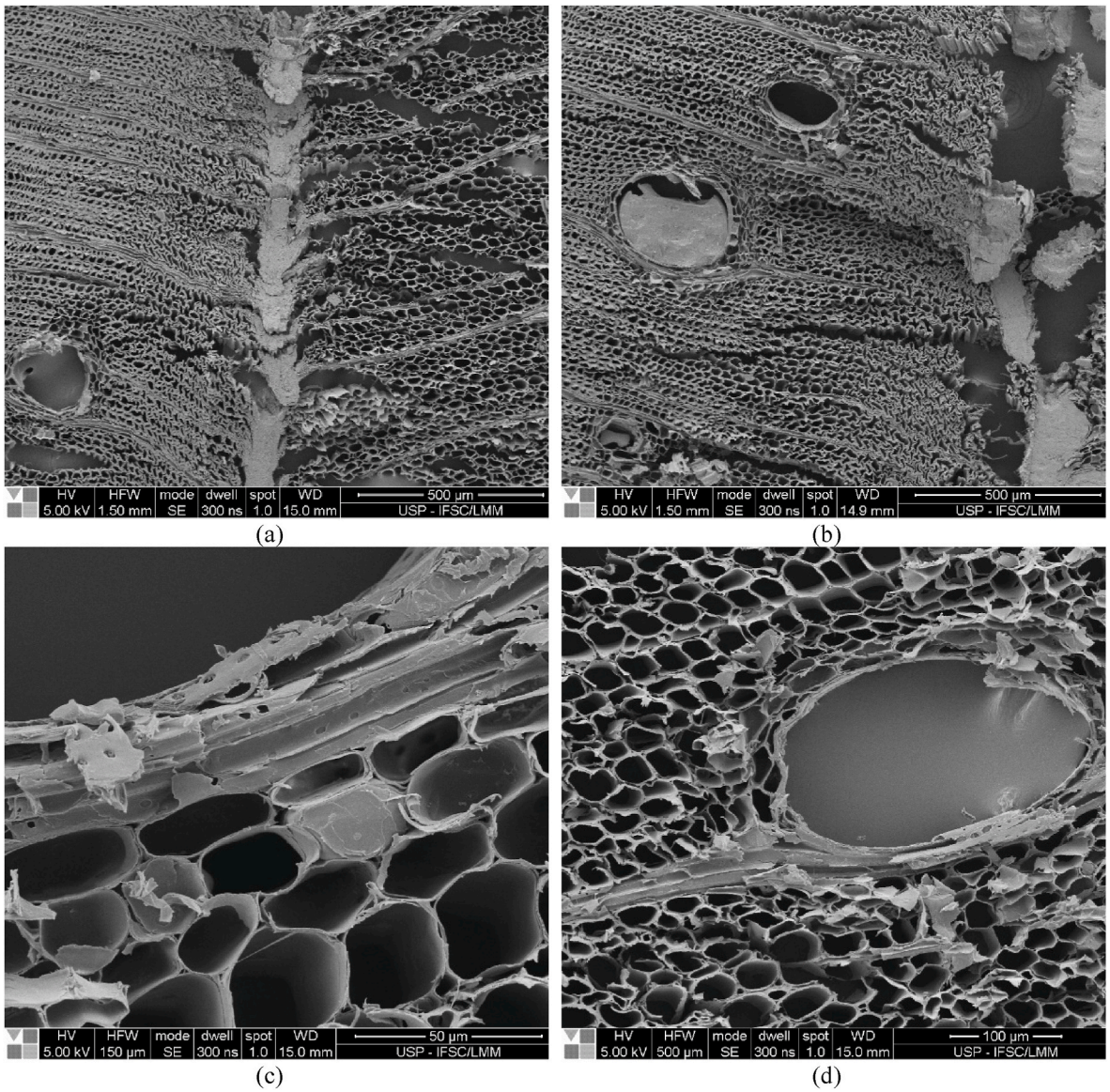

Fig. 13. SEM analysis of MUF bondline: overview of the adhesive bondline (a) detail of the damage to the sample (b) cellular wall detail (c) and filled ray detail (d).

shown in Fig. 4. In the sample with PU adhesive (Fig. 6) the lamellae displayed more similar interfaces in terms of tracheid diameter, even though they were bonded with different grain orientations.

The physicochemical properties of the adhesives must also be considered: the lower molecular weight of MUF confers greater mobility, favoring thinner and more uniform adhesive layers, whereas PU, with its higher molecular weight and viscosity, tends to form thicker lines [44]. These findings support observations from previous studies on similar adhesive systems in tropical woods, reinforcing the influence of the adhesive type, pressing protocol, and wood microstructure on the final morphology of the glue line [5,8,11]. Leggate et al. [28] demonstrated that both adhesive type and wood species significantly influence the thickness and continuity of the adhesive line, with previously planned surfaces and moderate pressing pressures leading to better results. Meanwhile, the study by Meethaworn, Srivaro and Khongtong [45] shows that anatomical features such as density and porosity directly impact adhesive distribution, requiring specific protocols for tropical woods.

It is worth noting that, based on the literature consulted, no studies were identified that present microscopic evaluations of the glue line in Paricá glulam beams directly comparable to those conducted in this work. The available investigations focus predominantly on macroscopic performance indicators, such as mechanical strength and delamination, which limits direct comparisons of microstructural parameters. In this context, the present study provides an initial reference by offering a microscopic characterization of the adhesive interface of this species, contributing to future comparative analyses in tropical woods.

4. Synthesis of the performance observed and recommended evaluation protocol

The results from the different microscopy techniques employed in this study clearly demonstrated the effective penetration of adhesives in the interface region between the lamellae of the glulam beams. Such penetration indicates that the sample surfaces exhibited suitable wettability and preparation conditions, resulting in robust adhesive bonds sufficient to integrate the structural elements [46,47].

Microstructural analyses revealed that the adhesive was able to fill not only the immediate region of the adhesive line, but also key anatomical elements of the wood, such as vessels and rays. These findings are in agreement with previous reports in the literature [16,48], which highlight that vessels, due to their larger diameter and the

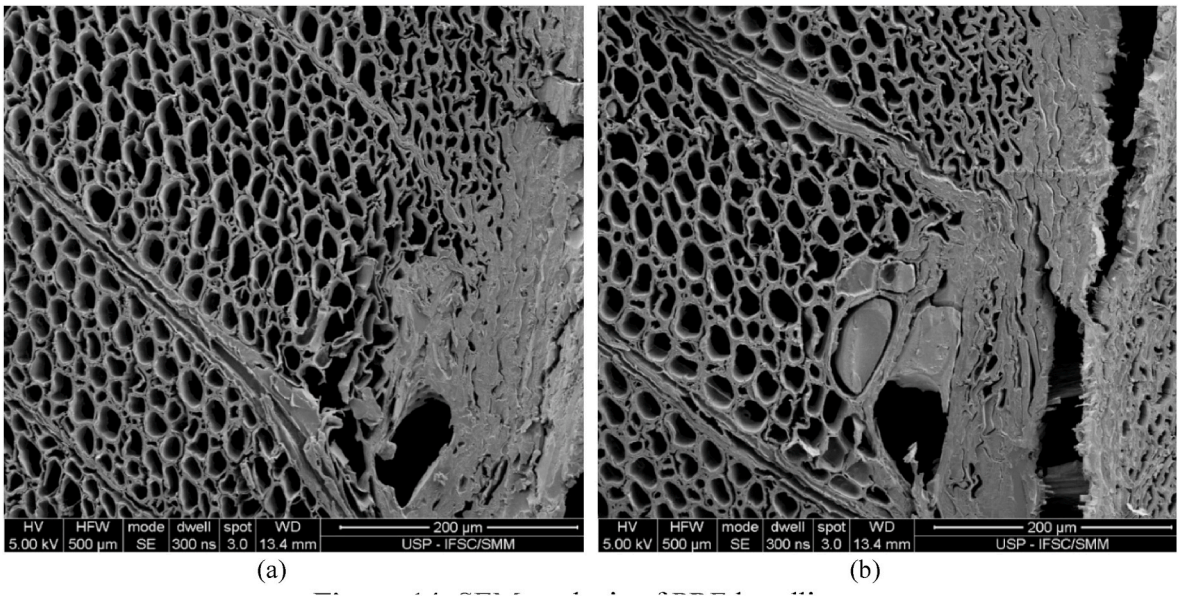

Fig. 14. SEM analysis of PRF bondline.

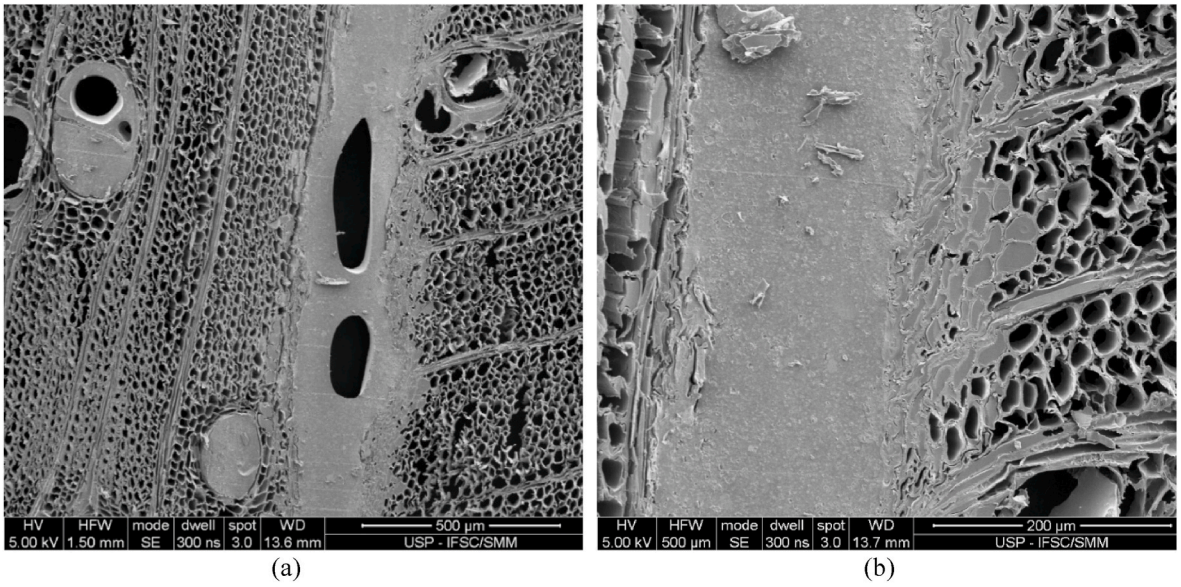

Fig. 15. SEM analysis of PU bondline: overview of the adhesive bondline (a) and detailed area of the bondline (b).

existence of intercellular perforations, act as preferential pathways for adhesive flow and anchorage. Since these elements are arranged in longitudinal series, forming long tunnels along the wood tissue, the adhesive is able to traverse long distances and anchor efficiently within the structure, explaining its presence even far from the pure adhesive line [49].

The rays, composed of parenchyma cells adapted for radial transport, also showed significant adhesive penetration, probably facilitated by the presence of transfer cells specialized in short-distance conduction. The study even showed the presence of adhesive in cell cavities adjacent to the adhesive line, which increases the depth and complexity of the bonding and suggests an efficient interaction between the polymer and the different classes of wood cells.

These findings reinforce that some macrostructural mechanical properties – such as modulus of elasticity (MOE), modulus of rupture (MOR), shear strength at the glue line, and delamination resistance – are direct consequences of phenomena observed at the microscopic scale. Thus, it becomes essential to integrate information from microstructural analyses with results from traditional tests to ensure truly comprehensive and predictive quality control for glulam elements.

It is also noteworthy that the evaluation of adhesive penetration requires a multi-technique approach. Only the combined use of different microscopy methods makes it possible to obtain comprehensive information about the adhesive bonding interfaces and associated mechanisms (according to Marra's model [50]). These techniques allow the assessment of features ranging from the morphology of the pure adhesive line to the identification of penetration patterns and, where applicable, semi-quantitative descriptors, as well as the characterization of the anatomical elements involved. It is important to note that the protocol proposed here is intended for micro-level quality assessment based on representative sampling from full-size glulam beams, rather than a full-field evaluation of adhesive penetration along the entire beam length.

Table 3 summarizes the main visualizations, advantages, and

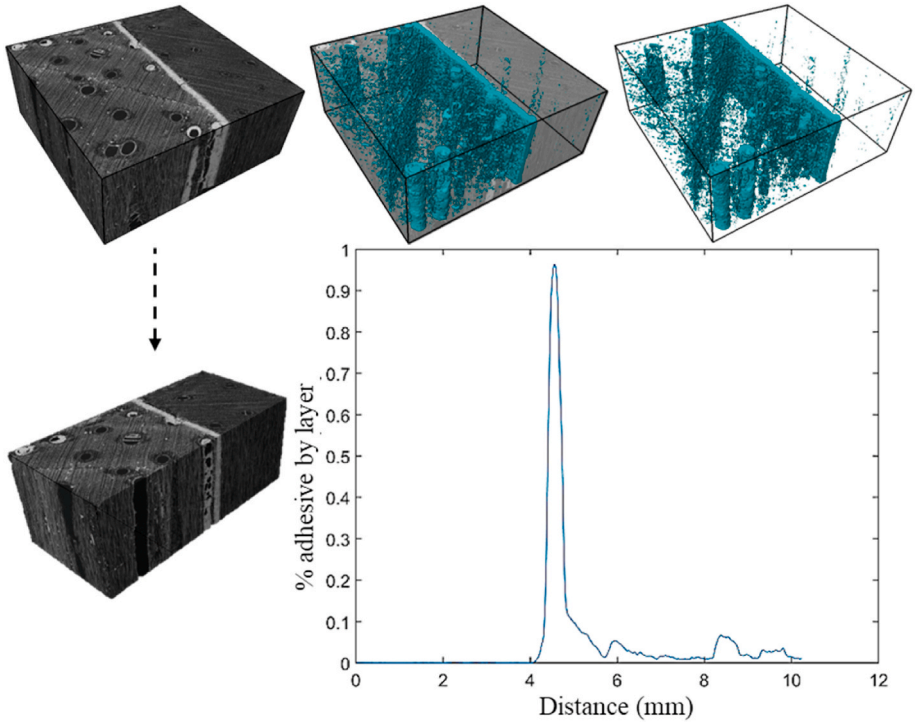

Fig. 16. MicroCT analysis of MUF bondline.

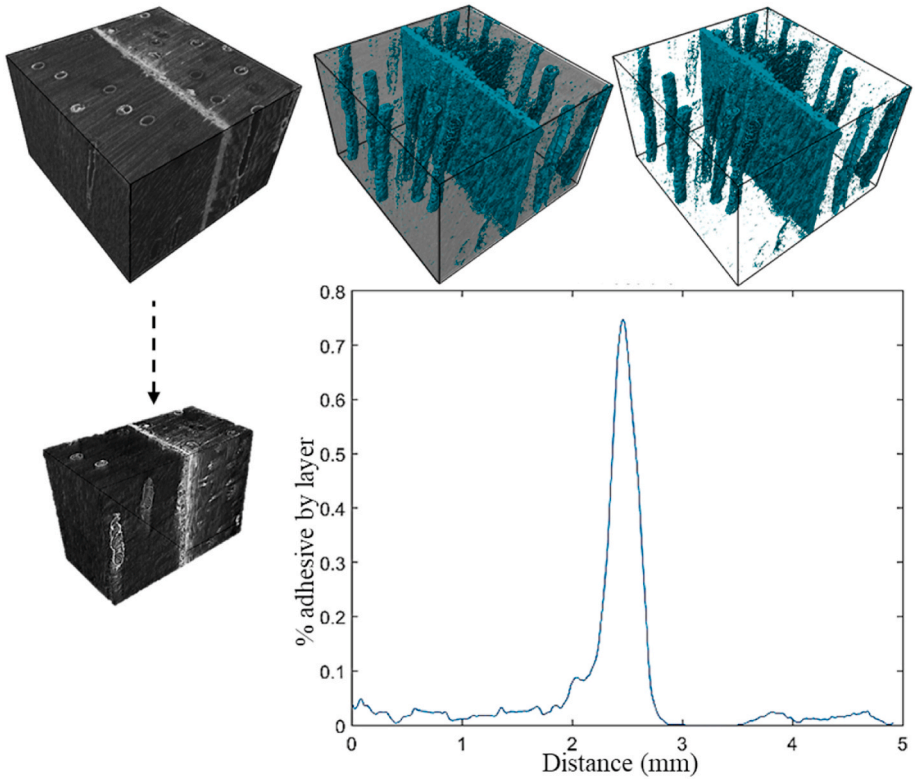

Fig. 17. MicroCT analysis of PRF bondline.

limitations of the microscopy techniques adopted in this study, serving as a reference for selecting the most appropriate methods for each analytical objective.

The results indicate that, due to the high intrinsic variability of the adhesive region, it is ideal to collect a representative sample: it is recommended to prepare six glulam beams bonded with the same wood species and adhesive, under identical manufacturing conditions. The ends at both extremities should be discarded, and at least three samples of 1 cm^3 should be taken from each adhesive line of each beam, at points distributed along its length.

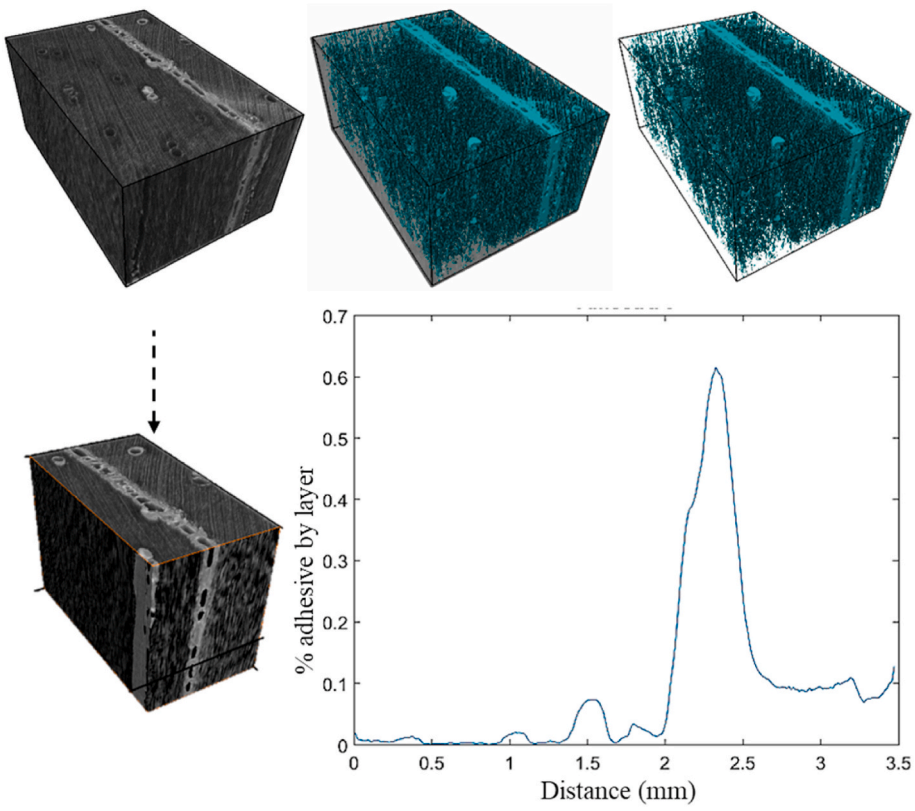

Fig. 18. MicroCT analysis of PU bondline.

Table 3
Comparison of the microscopy techniques used.

Technique	Visualization	Advantages	Disadvantages
LM	Pure adhesive line and anatomy	Identifies bubbles, crystals, and residual stress	Does not visualize penetration
FM	Pure adhesive line and rough penetration depth	Quick analysis, good contrast, identifies bubbles	Low focus/resolution (highly sensitive to section surface quality); requires fluorescent probe
CLSM	Pure adhesive line, rough penetration depth and cellular penetration	High resolution, excellent contrast, bubble identification	Shadows on irregular surfaces; uses probe
SEM	Lumen filling and glue line thickness	High resolution, bubble identification	Difficult to differentiate adhesive/timber (grayscale)
MicroCT	3D penetration (rough and cellular scale)	Non-destructive, high resolution, bubble identification	Requires adhesive contrast for high-density woods

The analysis of these samples should focus on the morphology of the pure adhesive line and on qualitative evidence of effective penetration at the interface. If future studies aim to statistically compare penetration-related parameters, replicated sampling along the beam length should be adopted to support robust inference. The sampling workflow illustrated in Fig. 19 is proposed as a practical starting point to support future standardization efforts in microscopic assessment of bondlines in engineered wood elements.

5. Conclusion

This study analyzed the adhesive lines of glulam samples produced with Paricá wood using three different adhesives and five microscopy techniques, allowing the distinction of the various regions of the adhesive interface and the evaluation of parameters such as adhesive penetration, line thickness, presence of preservatives, and anatomical elements of the wood tissue. Based on the results obtained, the following points can be highlighted.

- Satisfactory mechanical performance was achieved for all adhesive systems evaluated, with no delamination observed and failure occurring exclusively in the wood. These results confirm that the surface preparation, pressing conditions, and adhesive selection were appropriate, providing a reliable basis for the microstructural analysis of the adhesive interface.
- Microscopic analysis revealed clear differences in glue-line configuration depending on the adhesive type. MUF exhibited thinner and more uniform glue lines, associated with its lower molecular weight and higher mobility. PU produced thicker glue lines with the presence of bubbles, resulting from its expansion reaction. PRF showed intermediate behavior.
- When comparing the microscopy techniques, it was observed that:
  - oLM: proved suitable for rapid inspection of the pure adhesive line and identification of visible defects (bubbles, discontinuities), but without the ability to assess penetration.
  - oFM: allowed a preliminary estimation of glue-line thickness and penetration, though with severe limitations in focus and resolution.
  - oCLSM: was the most efficient technique for detailed analysis of the interface and penetration at the cellular level, offering high resolution and contrast.
  - oSEM: enabled precise observation of glue-line morphology and lumen filling, although with limitations in phase differentiation due to grayscale imaging and sensitivity to sample preparation.

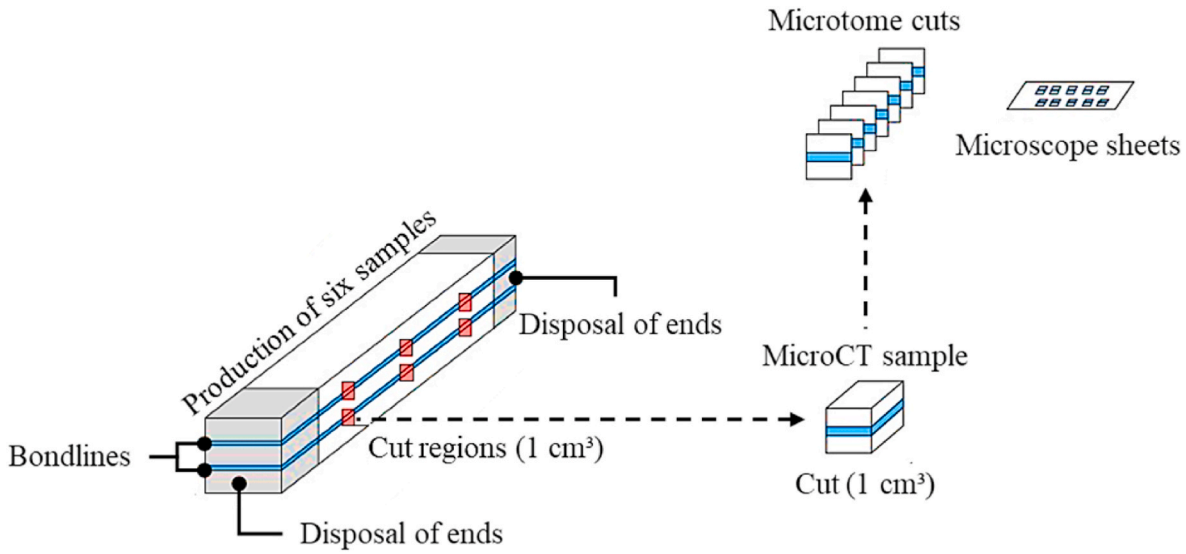

Fig. 19. Cutting protocol for obtaining samples for microscopic analysis of the bondline.

omicroCT: stood out for non-destructive three-dimensional visualization of adhesive distribution, being particularly relevant for volumetric analyses and assessment of glue-line continuity.

The results demonstrate that microscopic analyses provide complementary and indispensable information to conventional mechanical tests, allowing a deeper understanding of bonding mechanisms. For industrial applications, the use of at least two complementary techniques is recommended, selected according to the evaluation objective and production scale.

- Small and medium-sized glulam producers and routine inspection/visible defect control: LM combined with FM, due to their accessibility and rapid application. These techniques allow inspection of the pure adhesive line, identification of visible defects, and a preliminary estimation of adhesive penetration.
- Large companies and industrial centers with greater technological availability: the combined use of CLSM and SEM is recommended, particularly for product development, validation of new adhesives, or process optimization.
- Applied research or situations requiring advanced technological control: the use of microCT is recommended, as it enables non-destructive three-dimensional visualization, although it requires more advanced infrastructure.

Further work is also recommended to optimize specimen preparation (sectioning and surface quality), minimizing micro-damage that may limit the resolution of optical and SEM observations. Considering the variability present in the adhesive region, it is recommended that the sampling protocol presented here be adopted as a reference for future microscopic testing standards in engineered wood elements.

Data availability statements

Data sets generated during the current study are available from the corresponding author on reasonable request.

Declaration of competing interest

The authors declare that they have no known competing financial interests or personal relationships that could have appeared to influence the work reported in this paper.

Acknowledgments

The research would like to acknowledge the Coordenação de Aperfeiçoamento de Pessoal de Nível Superior, Brazil (CAPES).

References

[1] Dinwoodie JM. Timber: its nature and behaviour. second ed. London: E & FN Spon; 2004.
[2] Gomes NB, Jardim PILG, Christoforo AL, Souza AJD de, Molina JC. Análise dos parâmetros de fabricação de elementos de madeira lamelada colada na resposta da qualidade de colagem com base na NBR 7190-6. Ambient Construído 2025;25. https://doi.org/10.1590/s1678-86212025000100786.
[3] Rosa Talitha Oliveira, Terezo Rodrigo Figueiredo, Mascia Nilson Tadeu, Righez João Laryan Borges. Glued laminated timber of Paricá reinforced with synthetic fibers. Floresta, Curitiba 2019;49(3):459–68. https://doi.org/10.5380/rf.v49i3.59114.
[4] Zangiacomo A, Balanco G, Christoforo A, Lahr F. Glued laminated timber produced with tropical Brazilian wood species. Curr J Appl Sci Technol 2017;23:1–12. https://doi.org/10.9734/cjast/2017/34690.
[5] Oliveira KA de, Jardim PILG, Oliveira CAB, Rodrigues EFC, Christoforo AL, Molina JC. Assessment of the bonding quality of Toona ciliata (Australian cedar) lamellas for glulam beams produced with different adhesives and surface finishes. Int J Adhes Adhes 2025;138:103887. https://doi.org/10.1016/j.ijadhadh.2024.103887.
[6] Almeida DH de, Scaliante R de M, Macedo LB de, Macêdo AN, Dias AA, Christoforo AL, et al. Caracterização completa da madeira da espécie amazônica Paricá (Schizolobium amazonicum Herb) em peças de dimensões estruturais. Rev Arvore 2013;37:1175–81. https://doi.org/10.1590/S0100-67622013000600019.
[7] Vidaurre GB, Carneiro A de CO, Vital BR, dos Santos RC, Valle MLA. Propriedades energéticas da madeira e do carvão de paricá (Schizolobium amazonicum). Rev Arvore 2012;36:365–71. https://doi.org/10.1590/S0100-67622012000200018.
[8] Terezo RF, Szücs CA. Análise de desempenho de vigas em madeira laminada colada de parica (Schizolobium Amazonicum Huber ex. Ducke). Sci Sci 2010:471–80.
[9] Almeida DH De, Scaliante RDM, Macedo LB de, Macêdo AN, Calil C. Madeira laminada colada (MLC) da espécie Paricá. Madeira Arquitetura e Eng 2011;12:71–82.
[10] Cavalheiro RS, Calil Neto C, Christoforo AL, Calil Junior C, Lahr FAR. Evaluation of shear strength and cyclic delamination of paricá (Schizolobium amazonicum) glued laminated timber. Int J Mater Eng 2016;6:60–5. https://doi.org/10.5923/j.ijme.20160602.07.
[11] Almeida DH de, Cavalheiro RS, Macêdo LB de, Calil Neto C, Christoforo AL, Calil Junior C, et al. Evaluation of quality in the adhesion of glued laminated timber (Glulam) of paricá and lyptus wood species. Int J Mater Eng 2014;4:114–8. https://doi.org/10.5923/j.ijme.20140403.07.
[12] Terezo RF, Córdova FO De, Cadp Sampaio. Chemically treated glued laminated paricá timber (Schizolobium parahyba var. amazonicum). Eng Agríc 2019;39:158–65. https://doi.org/10.1590/1809-4430-eng.agric.v39n2p158-165/2019.
[13] Rosa TO, Terezo RF, Rios PDA, Sampietro JA, Rosa GO. Schizolobium Parahyba var. Amazonicum glulam classified by non-destructive tests. Floresta e Ambient 2019;26. https://doi.org/10.1590/2179-8087.120217.
[14] Rosa TO, Terezo RF, Mascia NT, Righez JLB. Glued laminated timber of paricá reinforced with synthetic fibers. FLORESTA 2019;49:459. https://doi.org/10.5380/rf.v49i3.59114.

[15] Terezo RF, Rosa TO, Furtado FRC, Ampessan CGM, Cunha AB, Do Valle A. Scarf joints in glued laminated timber of paricá. FLORESTA 2021;51:713. https://doi.org/10.5380/rf.v51i3.72445.
[16] Paris JL, Kamke FA. Quantitative wood-adhesive penetration with X-ray computed tomography. Int J Adhes Adhes 2015;61:71–80. https://doi.org/10.1016/j.ijadhadh.2015.05.006.
[17] Musah M, Wang X, Dickinson Y, Ross RJ, Rudnicki M, Xie X. Durability of the adhesive bond in cross-laminated northern hardwoods and softwoods. Constr Build Mater 2021;307:124267. https://doi.org/10.1016/j.conbuildmat.2021.124267.
[18] Cheng RX, Gu JY. Study on bonding properties of Larch with WPI adhesive. Pigment Resin Technol 2010;39:359–64. https://doi.org/10.1108/03699421011085867.
[19] Qin L, Lin L, Fu F. Microstructural and micromechanical characterization of modified urea-formaldehyde resin penetration into wood. Bioresources 2016;11:182–94. https://doi.org/10.15376/biores.11.1.182-194.
[20] Molina JC, Bianchi NA, Lisboa FD, Gomes NB. Collage quality of Brazilian woods for use in glued laminated timber beams. 13th World Conf Timber Eng WCTE 2023 2023;2:729–34. https://doi.org/10.52202/069179-0100.
[21] Núñez-Decap M, Pérez-Soto G, Opazo-Vega A, Moya-Rojas B, Vidal-Vega M. Study of wood adhesives on the bonding properties in solid and hollow glulam beams of Pinus Radiata. Wood Res 2022;67:598–611. https://doi.org/10.37763/wr.1336-4561/67.4.598611.
[22] Liu J, Yue K, Xu L, Wu J, Chen Z, Wang L, et al. Bonding performance of melamine-urea–formaldehyde and phenol-resorcinol–formaldehyde adhesive glulams at elevated temperatures. Int J Adhes Adhes 2020;98. https://doi.org/10.1016/j.ijadhadh.2019.102500.
[23] Yang L, Chen A, Zhou J, He G, Wang H, Li C. Flexural fatigue behavior of Glulam beams connected with steel splints and bolts. Buildings 2023;13:1218. https://doi.org/10.3390/buildings13051218.
[24] Qu J, Gong Y, Li M, Ren H. Evolution of interlaminar shear failure in CLT: insights from theoretical calculation, acoustic emission, and microstructural analysis. Constr Build Mater 2025;470. https://doi.org/10.1016/j.conbuildmat.2025.140510.
[25] Wang SM, Shi J you, Xu W. Synthesis and characterization of starch-based aqueous polymer isocyanate wood adhesive polymer isocyanate wood adhesive. Bioresources 2015;10:7653–66. https://doi.org/10.15376/biores.10.4.7653-7666.
[26] Wang VZ, Ginger JD, Narayan K. Intralaminar and interlaminar fracture characterization in glued-laminated timber members using image analysis. Eng Fract Mech 2012;82:73–84. https://doi.org/10.1016/j.engfracmech.2011.11.024.
[27] Gao Z, Wang W, Zhao Z, Guo M. Novel whey protein-based aqueous polymer-isocyanate adhesive for glulam. J Appl Polym Sci 2011;120:220–5. https://doi.org/10.1002/app.33025.
[28] Leggate W, Shirmohammadi M, McGavin RL, Outhwaite A, Knackstedt M, Brookhouse M. Examination of wood adhesive bonds via MicroCT: the influence of pre-gluing surface machining treatments for Southern pine, spotted gum, and Darwin stringybark timbers. Bioresources 2021;16:5058–82. https://doi.org/10.15376/biores.16.3.5058-5082.
[29] Böger T, Engelhardt M, Suh FT, Richter K, Sanchez-Ferrer A. Wood-water interactions of primers to enhance wood-polyurethane bonding performance. Wood Sci Technol 2024;58:135–60. https://doi.org/10.1007/s00226-023-01508-z.
[30] Momentive. Cascophen R7132/Cascoset MCAT 9131: technical data sheet. 2012. p. 1–7.
[31] Lei H, Frazier CE. Curing behavior of melamine-urea-formaldehyde (MUF) resin adhesive. Int J Adhes Adhes 2015;62:40–4. https://doi.org/10.1016/j.ijadhadh.2015.06.013.
[32] Associação Brasileira de Normas Técnicas. NBR 7190-2: projeto de estruturas de madeira. Parte 2 - métodos de ensaio para classificação visual e mecânica de peças estruturais de madeira. Rio de Janeiro: ABNT; 2022.
[33] Canadian Standards Association. Csa O112.9: evaluation of adhesives for structural wood products. CSA; 2021.
[34] Glišović I, Stevanović B, Todorović M. Flexural reinforcement of glulam beams with CFRP plates. Mater Struct Constr 2016;49:2841–55. https://doi.org/10.1617/s11527-015-0690-7.
[35] Gavrilović-Grmuša I, Dunky M, Miljković J, Djiporović-Momčilović M. Influence of the degree of condensation of urea-formaldehyde adhesives on the tangential penetration into beech and fir and on the shear strength of the adhesive joints. Eur J Wood Wood Prod 2012;70:655–65. https://doi.org/10.1007/s00107-012-0599-6.
[36] Calil Neto C, Christoforo AL, Ribeiro Filho SLM, Lahr FAR, Calil Júnior C. Avaliação da resistência ao cisalhamento e à delaminação em madeira laminada colada. Cienc Florest 2014;24.
[37] Segundinho PG de A, Zangiácomo AL, Carreira MR, Dias AA, Lahr FAR. Avaliação de vigas de madeira laminada colada de cedrinho (Erisma uncinatum Warm.). Cerne 2013;19:441–9. https://doi.org/10.1590/S0104-77602013000300011.
[38] Segundinho PG de A, Gonçalves FG, Gava GC, Tinti VP, Alves SD, Regazzi AJ. Eficiência da colagem de madeira tratada de Eucalyptus cloeziana F. Muell para produção de madeira laminada colada (MLC). Materia 2017;22. https://doi.org/10.1590/s1517-707620170002.0140.
[39] European Committee for Standardization (CEN). BS EN 386: glued laminated timber - performance requirements and minimum production requirements. Brussels: CEN; 2001.
[40] Associação Brasileira de Normas Técnicas (ABNT). NBR 7190-6: projeto de estruturas de madeira parte 6 - métodos de ensaio para caracterização de madeira lamelada colada estrutural. Rio de Janeiro: ABNT; 2022.
[41] Câmpu RV, Derczeni RA. European beech log sawing using the small-capacity band saw: a case Study on time consumption, productivity and recovery rate. Forests 2023;14:1137. https://doi.org/10.3390/f14061137.
[42] Monteiro TC, Lima JT, Silva JRM da, Trugilho PF, Andrade BCL de. Avaliação do desdobro de toras de Eucalyptus para a obtenção de peças estruturais. Cerne 2013;19:357–64. https://doi.org/10.1590/S0104-77602013000300001.
[43] Silva LFM, Öchsner A, Adams RD. Handbook of adhesion technology. second ed. Cham: Springer International Publishing; 2018. https://doi.org/10.1007/978-3-319-55411-2.
[44] Ferdosian F, Pan Z, Gao G, Zhao B. Bio-based adhesives and evaluation for wood composites application. Polymers 2017;9:70. https://doi.org/10.3390/polym9020070.
[45] Meethaworn B, Srivaro S, Khongtong S. High-performance adhesive joint made from DensifiedWood. Polymers 2022;14. https://doi.org/10.3390/polym14030515.
[46] Chandler JG, Brandon RL, Frihart CR. Examination of adhesive penetration in modified wood using fluorescence microscopy. ASC Spring 2005 Conv Expo April 2005;c:17–9.
[47] Chandler JG, Frihart CR. Assessment of increased wet wood bonding for epoxy-bonded samples using a melamine-urea-formaldehyde priming agent. Wood Adhes, San Diego: The USDA Forest Service, Forest Products Laboratory 2005:99–106.
[48] Paris JL, Kamke FA, Mbachu R, Gibson SK. Phenol formaldehyde adhesives formulated for advanced X-ray imaging in wood-composite bondlines. J Mater Sci 2014;49:580–91. https://doi.org/10.1007/s10853-013-7738-2.
[49] Albino VC do S, Mori FA, Mendes LM. A study of the bonding of wood from Eucalyptus grandis W. Hill ex Maiden using resorcinol-formaldehyde adhesive. Cerne 2010;16:443–9. https://doi.org/10.1590/S0104-77602010000400003.
[50] Marra AA. Technology of wood bonding: principles and practice. New York: Van Nostrand Reinhold; 1992.